NASA/TM-2009-215715

The Development of Directional Decohesion Finite Elements for Multiscale Failure Analysis of Metallic Polycrystals

Erik Saether and Edward H. Glaessgen
Langley Research Center, Hampton, Virginia

April 2009

NASA STI Program . . . in Profile

Since its founding, NASA has been dedicated to the advancement of aeronautics and space science. The NASA scientific and technical information (STI) program plays a key part in helping NASA maintain this important role.

The NASA STI program operates under the auspices of the Agency Chief Information Officer. It collects, organizes, provides for archiving, and disseminates NASA's STI. The NASA STI program provides access to the NASA Aeronautics and Space Database and its public interface, the NASA Technical Report Server, thus providing one of the largest collections of aeronautical and space science STI in the world. Results are published in both non-NASA channels and by NASA in the NASA STI Report Series, which includes the following report types:

- TECHNICAL PUBLICATION. Reports of completed research or a major significant phase of research that present the results of NASA programs and include extensive data or theoretical analysis. Includes compilations of significant scientific and technical data and information deemed to be of continuing reference value. NASA counterpart of peer-reviewed formal professional papers, but having less stringent limitations on manuscript length and extent of graphic presentations.

- TECHNICAL MEMORANDUM. Scientific and technical findings that are preliminary or of specialized interest, e.g., quick release reports, working papers, and bibliographies that contain minimal annotation. Does not contain extensive analysis.

- CONTRACTOR REPORT. Scientific and technical findings by NASA-sponsored contractors and grantees.

- CONFERENCE PUBLICATION. Collected papers from scientific and technical conferences, symposia, seminars, or other meetings sponsored or co-sponsored by NASA.

- SPECIAL PUBLICATION. Scientific, technical, or historical information from NASA programs, projects, and missions, often concerned with subjects having substantial public interest.

- TECHNICAL TRANSLATION. English-language translations of foreign scientific and technical material pertinent to NASA's mission.

Specialized services also include creating custom thesauri, building customized databases, and organizing and publishing research results.

For more information about the NASA STI program, see the following:

- Access the NASA STI program home page at *http://www.sti.nasa.gov*

- E-mail your question via the Internet to help@sti.nasa.gov

- Fax your question to the NASA STI Help Desk at 443-757-5803

- Phone the NASA STI Help Desk at 443-757-5802

- Write to:
  NASA STI Help Desk
  NASA Center for AeroSpace Information
  7115 Standard Drive
  Hanover, MD 21076-1320

NASA/TM-2009-215715

The Development of Directional Decohesion Finite Elements for Multiscale Failure Analysis of Metallic Polycrystals

Erik Saether and Edward H. Glaessgen
Langley Research Center, Hampton, Virginia

National Aeronautics and
Space Administration

Langley Research Center
Hampton, Virginia 23681-2199

April 2009

Available from:

NASA Center for AeroSpace Information
7115 Standard Drive
Hanover, MD 21076-1320
443-757-5802

Table of Contents

Abstract

Atomistic simulations of intergranular fracture have indicated that grain-scale crack growth in polycrystalline metals can be direction dependent. At these material length scales, the atomic environment greatly influences the nature of intergranular crack propagation, through either brittle or ductile mechanisms, that are a function of adjacent grain orientation and direction of crack propagation. Methods have been developed to obtain cohesive zone models (CZM) directly from molecular dynamics simulations. These CZMs may be incorporated into decohesion finite element formulations to simulate fracture at larger length scales. A new directional decohesion element is presented that calculates the direction of Mode I opening and incorporates a material criterion for dislocation emission based on the local crystallographic environment to automatically select the CZM that best represents crack growth. The simulation of fracture in 2-D and 3-D aluminum polycrystals is used to illustrate the effect of parameterized CZMs and the effectiveness of directional decohesion finite elements.

1. Introduction

At nanometer length scales, the local atomic environment greatly influences the nature of intergranular crack propagation. Crack tip process zones can be characterized by brittle or ductile mechanisms that are initiated as a function of adjacent grain orientation and direction of crack propagation. Experimental evidence for the crystallographic dependence of crack tip processes date back to the work of Bilby and Bullough (1954). The atomistic response at the crack front can be obtained through molecular dynamics (MD) simulation and cast into an aggregate traction-displacement relationship and subsequently used as part of a sequential multiscale analysis (Yamakov et al., 2006; Saether, 2008).

Sequential multiscale modeling typically involves some form of averaging of physical parameters that can serve as initial conditions or provide material parameters to another model which is analyzed separately. A desirable aspect of sequential methods is that length and time scales between independent material models do not have to be coupled. The averaging or homogenization of information across length scales that is inherent to sequential multiscale methods is depicted in Figure 1 where a notional coupling is shown across domains representing characteristic features at the sub-atomic through structural length scales.

Cohesive zone models (CZM) are based on traction-displacement relationships and are a viable tool for sequential multiscale modeling (Saether, 2008). Within a sequential analysis framework, CZMs based on averaged atomistic deformation processes for intergranular and transgranular fracture can be used to simulate material behavior at larger length scales.

The notional flow of sequential coupling that utilizes CZMs to carry information of microscopic failure mechanisms to predict damage progression at larger length scales is depicted in Figure 2. Hitherto, the properties of the CZM have been determined empirically or heuristically, and mixed-mode fracture has been limited to empirical relationships that have been applied at both microscopic and macroscopic length scales.

In Figure 2, CZMs provide the critical transition between inherently atomistic and inherently continuum representations.

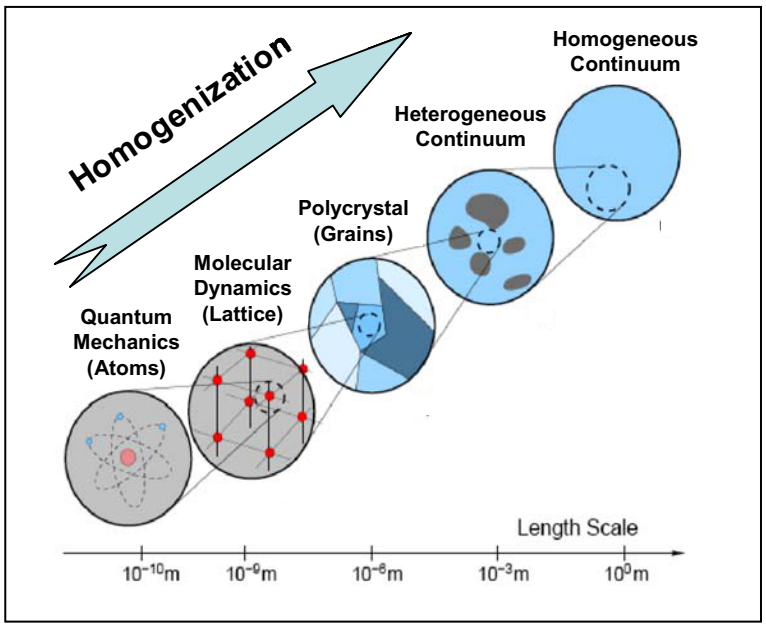

Figure 1. Hierarchy of models over length scales from quantum mechanical through homogeneous continuum. (Adapted from Oden et al., 2006)

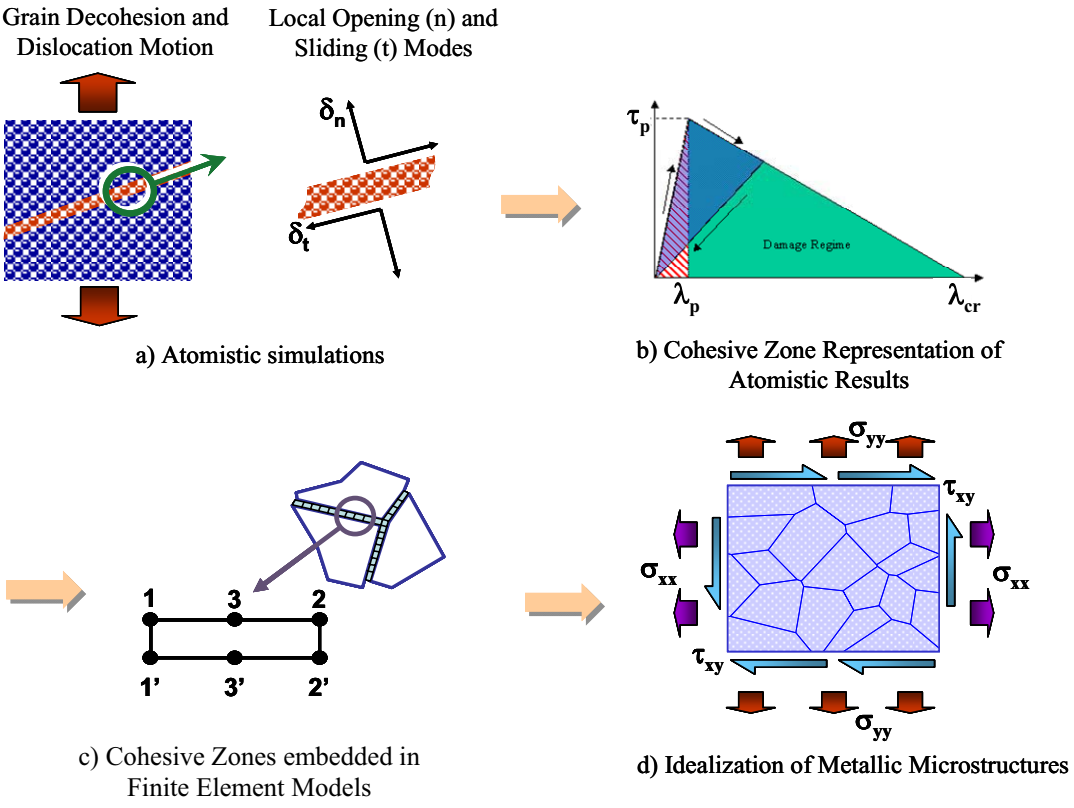

Figure 2. Multiscale analysis with cohesive zone models.

Characterization of intergranular fracture for different grain boundary (GB) orientations is currently very limited. Yamakov et al. (2006) determined CZM parameters for intergranular fracture of a symmetric tilt Σ99 GB, which, depending on the direction of propagation, exhibited either ductile or brittle fracture characteristics in Mode I opening. With the lack of predictions of CZM parameters for other GB orientations, scaling the results obtained by Yamakov et al. (2006) for fracture along a single GB is used in the current study to represent other GB orientations.

CZMs may be incorporated into decohesion finite element formulations to simulate fracture at continuum length scales. The CZMs provide constitutive relations that govern the separation of material planes due to relative displacement measures that correspond to the three fundamental modes of fracture. A new feature to decohesion finite element formulations is presented that allows the element to automatically apply appropriate brittle or ductile CZMs for crack growth depending on the direction of fracture propagation. This new feature thus modifies the element behavior as the finite element analysis proceeds.

Six-node and 12-node directional decohesion finite elements are formulated that incorporate Rice's criterion (Rice, 1992) for dislocation emission to automatically select the appropriate CZM to simulate brittle or ductile crack propagation characteristics. For intergranular fracture, element input requires the crystallographic orientation of the adjacent grains in the microstructure and additional material parameters including surface, GB, stable and unstable stacking-fault, and unstable twinning energy in order to predict brittle or ductile Mode I fracture.

Section 2 presents a general discussion of cohesive zone models, and Section 3 presents an overview of decohesion element formulations. Specific formulations of directional decohesion elements are detailed in Section 3.1. Finally, Section 4 presents illustrative simulations of intergranular fracture in 2-D and 3-D aluminum polycrystal models. A 2-D model is used to demonstrate the effect of CZM parameterization, and two

3-D models are used to assess the unique modeling capability of directional decohesion finite elements.

2. Cohesive Zone Models

Cohesive zone models were originally developed to represent complicated nonlinear fracture processes in ductile and quasi-brittle materials (Dugdale, 1960; Barenblatt, 1962). CZMs were later developed to describe general adhesion and frictional slip along an interface (Maugis, 1992; Kem et al., 1998). The CZM approach is formulated from a constitutive relationship based on applied tractions and relative displacements to represent separation in various fracture modes of two initially coincident and bonded internal surfaces. The relative displacements associated with the creation of a new fracture surface for the three fundamental fracture modes are depicted in Figure 3.

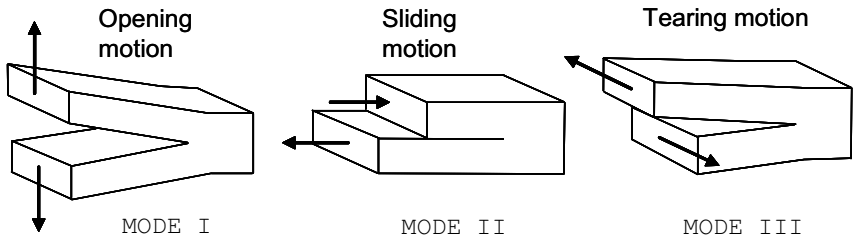

Figure 3. Fundamental fracture modes in solids

In a CZM-based approach, the area under the CZM traction-displacement curve represents the work of separation to open a crack in a particular fracture mode, i.e. the fracture toughness, and is given by Tvergaard and Hutchinson (1992) as

$$G_c = \int_0^{\Delta^f} \tau d\Delta \tag{1}$$

where G_c is the work of separation, τ is the applied traction, Δ is a general form of the displacement, and Δ^f is the critical displacement at which complete separation has occurred and the tractions are zero.

In general, the traction-displacement relationships $\tau(\Delta)$ are obtained through differentiation of a potential $\phi=\phi(\Delta)$, which represents the free energy of decohesion. The selection of a potential function is typically based on recovering the assumed traction-displacement relationship, and particular forms are generally selected for analytical convenience. In practice, various forms have been used as shown in Table 1. The existence of a work potential yields the work of separation as independent of the loading history and of the specific shape of the traction-displacement law.

Cohesive properties along an interface have typically been approximated using empirical data to define the CZMs (Tvergaard and Hutchinson, 1992; Costanzo and Allen, 1995; Camacho and Ortiz, 1996; Klein and Gao, 1998; Zavattieri et al., 2001; Zavattieri and Espinosa, 2003; Turon et al., 2004). These models are frequently used in conjunction with the finite element method (FEM) to study fracture at macroscopic length scales in a wide variety of materials.

The shape of the CZM law represents the behavior of the material near the crack tip under load. Various attempts have been made to determine the shape based on fundamental bonding characteristics in metals (Rose et al., 1983; Nguyen and Ortiz, 2002). The most commonly assumed forms of the traction-displacement law have been expressed as exponential, bilinear, and trapezoidal functions. A general review of various forms of CZMs is presented by Chandra et al. (2002) and summarized in Table 1. The table illustrates the basic form of the CZMs, their key parameters, and important features.

Table 1. Various cohesive zone models and their parameters. (From Chandra et al., 2002)

Author (year)	Proposed model	Model parameters	Problem solved	Model constants	Comments
Barenblatt (1959, 1962)	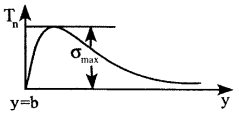	$K = \int_0^{d+d'} \frac{G_1(t)\,dt}{\sqrt{t}}$ $= \sqrt{\frac{\pi E T}{1-\nu^2}}$ (ductile) $= \sqrt{\frac{\pi E T_0}{1-\nu^2}}$ (brittle) $T = T_0 + T_1$ T_0 is work of separation for brittle materials T_1 is work of plastic deformation	Perfectly brittle materials		The first to propose the cohesive zone concept
Dugdale (1960)	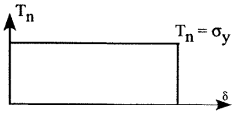	$\frac{s}{a} = 2\sin^2\left(\frac{\pi}{4}\frac{T}{\sigma_y}\right)$ For small value of T/σ_y $\frac{s}{l} = 1.23\left(\frac{T}{\sigma_y}\right)^2$	Yielding of thin ideal elastic–plastic steel sheets containing slits	Plastic zone ranges from 0.042 to 0.448 (in.)	Cohesive stress equated to yield stress of material
Needleman (1987)	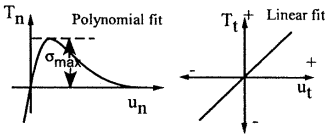	ϕ_{sep} is work of separation δ are normalizing parameters σ_{max} is cohesive strength	Particle-matrix decohesion	$\delta = 10^{-9}$ to 10^{-8} m cohesive energy 1–10 J/m^2 $\sigma_{max} = 1000$–1400 MPa $\sigma_y = 350$–450 MPa	Phenomenological model; predicts normal separation
Rice and Wang (1989)	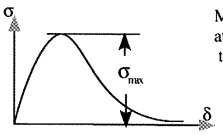	E_0 is initial Young's modulus h is normalizing parameter σ_{max} is maximum stress α is constant $\left(\frac{E_0 h}{2^2} = 2\gamma\right)$	Solute segregation		Ascending part is equated to E_0 considers normal separation and ignores shear separation
Needleman (1990a)	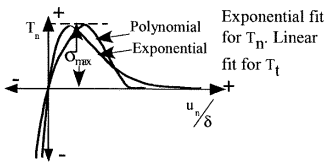	ϕ_{sep} is work of separation δ are normalizing parameters σ_{max} is cohesive strength	Particle-matrix decohesion	$\delta = 10^{-9}$ to 10^{-8} m	Predicts normal separation
Needleman (1990b)	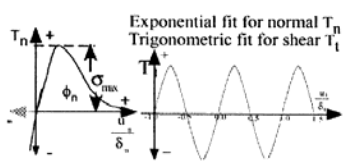	ϕ_n, ϕ_t are work of normal and shear separation δ_n, δ_t are critical displacements σ_{max} is cohesive strength	Decohesion of interface under hydrostatic tension	$\delta_n = \delta_t = 2 \times 10^{-10}$ to 2×10^{-9} m $J_{1C}/\phi_n = 0.57$–2.59 $\sigma_{max}/\sigma_0 = 2, 3$	Periodic shear traction to model Pieriels shear stress due to slip
Tvergaard (1990)	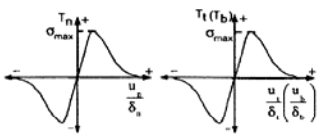	δ_n, δ_t are critical displacements σ_{max} is cohesive strength	Interfaces of whisker reinforced metal matrix composites	$\delta_n = \delta_t = 1 \times 10^{-9}$ m $E = 60$ GPa (Young's mod) $\sigma_y/E = 0.005$ $\sigma_{max}/\sigma_y = 5$–9	Quadratic model
Tvergaard and Hutchinson (1992)	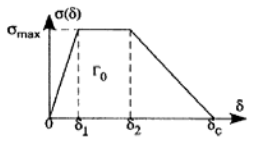	Γ_0 is work of separation δ_c is critical displacement σ_{max} is peak normal traction /interface strength δ_1, δ_2 are factors governing shape	Crack growth in elasto-plastic material, peeling of adhesive joints	$\Gamma_{ss}/\Gamma_0 = 0$–10 (Γ_{ss} = Pl wk.), $\delta_n^c/\delta_t^c = 1$ $\sigma_{max}/\sigma_y = 0$–14 δ_1, $\delta_2 = 0.15, 0.5$ $\sigma_y/E = 1/300$	Claims shape of separation law are relatively unimportant
Xu and Needleman (1993)	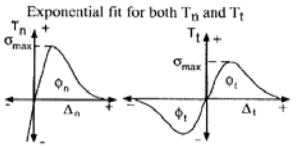	ϕ_n is work of normal separation ϕ_t is work of shear separation δ_n, δ_t are critical displacements σ_{max} is cohesive strength	Particle-matrix decohesion	$\delta_n = \delta_t = 2 \times 10^{-10}$ to 2×10^{-9} m	Predicts shear and normal separation

Despite all of the forms of CZMs that have been proposed, a commonly used mathematical form not shown in Table 1, is a bilinear constitutive relation. The bilinear form is often chosen because of its mathematical simplicity and its suitability for representing brittle and ductile fracture in metals (Yamakov et al., 2006), and purely brittle fracture in polymeric and ceramic composite materials (Camacho and Ortiz, 1996). Bilinear types of cohesive zone models have been used in several recent finite element simulations of brittle fracture during multi-axial dynamic loading of ceramic microstructures (Zavattieri et al., 2001, 2003). This form of a CZM is shown in Figure 4.

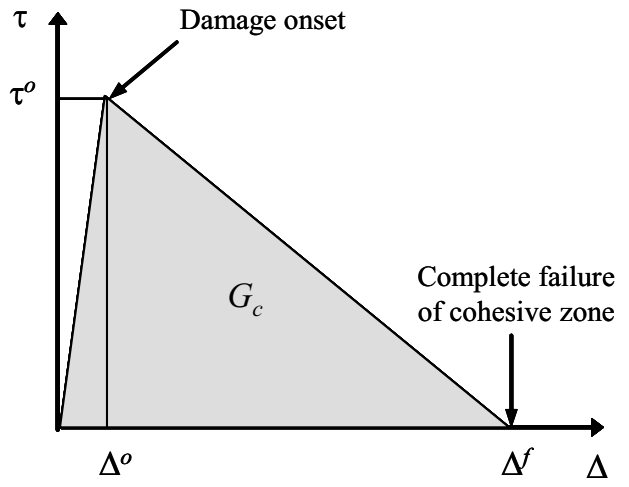

Figure 4. Bilinear cohesive zone model.

In Figure 4, Δ represents relative discontinuous displacement jumps between the upper and lower nodes, $\Delta = \Delta^{top} - \Delta^{bot}$. Δ^o indicates the displacement jump corresponding to the maximum traction and indicates the onset of damage. Final failure of the cohesive zone is assumed after the relative displacement jump yields zero traction. This maximum relative displacement jump is indicated as Δ^f.

An interpolation procedure using single-mode CZMs has been developed by Turon et al. (2004) to generate an effective CZM for mixed-mode applications. This interpolation or coupling scheme is depicted in Figure 5.

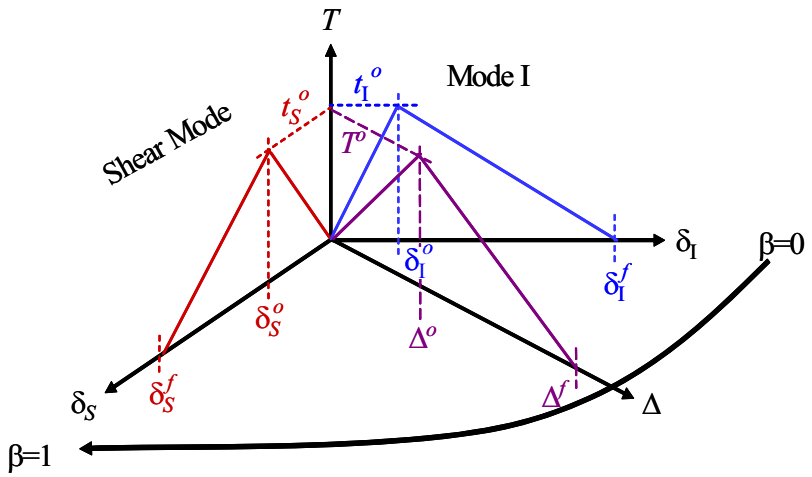

Figure 5. Interpolation of CZM components.

In Figure 5, the relative displacement jumps for single-mode CZMs are denoted by $\delta = \delta_{top} - \delta_{bot}$ while Δ refers to the interpolated displacement jumps. The interpolation of "normal" and "shear" CZMs to obtain a single effective CZM is made to represent mixed normal and tangential fracture modes. The Mode II and III displacements, δ_{II} and δ_{III}, are combined by the root sum of the squares to make a combined "shear" displacement,

$$\delta_S = \sqrt{(\delta_{II})^2 + (\delta_{III})^2} \tag{2}$$

and the coupled displacement across the interface is defined by

$$\Delta = \sqrt{\langle \delta_I \rangle^2 + (\delta_S)^2} \tag{3}$$

where $\langle\ \rangle$ is the MacAuley bracket function, $\langle x \rangle = \frac{1}{2}\left(x + |x|\right)$. Mode mixity parameters are defined by

$$\beta = \frac{\delta_S}{\delta_S + \langle \delta_I \rangle} \qquad B = \frac{\beta^2}{1 + 2\beta^2 - 2\beta} \tag{4}$$

where $\beta = 0$ for pure Mode I loading, and $\beta = 1$ for pure shear loading. The fracture onset criterion is defined by

$$\Delta^o = \sqrt{(\delta_I^o)^2 + \left[(\delta_S^o)^2 - (\delta_I^o)^2\right] B^\eta} \tag{5}$$

and the criterion for complete fracture representing crack propagation is derived from the B-K critical energy release rate expression (Benzeggagh and Kenane, 1996) given by

$$G_c = G_{Ic} + \left(G_{shear} - G_{Ic}\right)\left(\frac{G_{shear}}{G_{tot}}\right)^\eta \tag{6}$$

where $G_{tot} = G_I + G_{shear}$, $G_{shear} = G_{II} + G_{III}$, and η is an empirical factor used to correlate with experimental data. This leads to an expression for the final opening displacement jump corresponding to crack propagation given by

$$\Delta^f = \frac{\delta_I^o \delta_I^f + \left(\delta_S^o \delta_S^f - \delta_I^o \delta_I^f\right) B^\eta}{\Delta^o} \quad . \tag{7}$$

In the previous expressions, δ_I^f, δ_{II}^f, and δ_{III}^f are the individual nodal displacement jumps corresponding to opening in Mode I, II and III, respectively, and are user-specified. The δ_I^o, δ_{II}^o, and δ_{III}^o are the individual nodal displacements corresponding to the onset of damage and are computed from the user-specified initial stiffness values, k_I^o, k_{II}^o, and k_{III}^o, and peak tractions, t_I^o, t_{II}^o, and t_{III}^o, of the single-mode CZMs. The

interpolated parameters, Δ^o and Δ^f, define the mixed-mode CZM used in decohesion finite elements for the continuum simulation of fracture.

2.1 CZM Parameters Dependent on Direction of Crack Growth

Important damage and failure behavior in polycrystalline metals can be simulated including intergranular fracture along grain boundaries in metals, transgranular fracture along slip planes, and fracture through interfaces between grains and small second phase particles. At atomistic length scales, it has been shown that for a common Σ99 symmetric tilt GB, Mode I fracture can propagate by distinct ductile or brittle modes depending on the direction of propagation (Yamakov et al., 2006). A synopsis of the distinct directional difference in crack propagation behavior and the atomistic determination of corresponding CZM parameters as presented by Yamakov et al. (2006) is shown in Figure 6. The system was subjected to a hydrostatic tensile load in order to avoid shear stresses away from the crack that could induce undesired dislocation formation. To ensure crack nucleation and growth at the nanometer scale, the prestress in the range of 3.75 to 4.25 GPa was considered.

Figure 6 shows characteristics of the propagating internal crack at different times during a MD simulation. At t = 12 ps, the center crack shown at the top of the figure has well-developed differences in the crack tip behavior at the two ends. The left crack tip, highlighted at t = 68 ps, shows a large degree of blunting due to several formations that are identified as the development of twinning (②), cores of partial or twinning dislocations (③) and secondary slip (⑦). The right crack tip, shown at t = 55 ps, demonstrates cleavage associated with brittle fracture. The calculated CZM for ductile opening shows a peak traction of ~4.0 GPa and an expected large opening displacement for final fracture. For brittle fracture, the CZM is characterized by a peak traction of ~5.0 GPa and a shorter softening region prior to complete opening in Mode I. The CZM curves are computed as moving averages of traction-displacement measurements obtained from MD simulation (See Yamakov et al., 2006). In the CZM curves presented

in Figure 6, the individual data points and a least-squares curve fit for a prestress of 4.25 GPa are shown, together with curve fits for the other magnitudes of applied prestress.

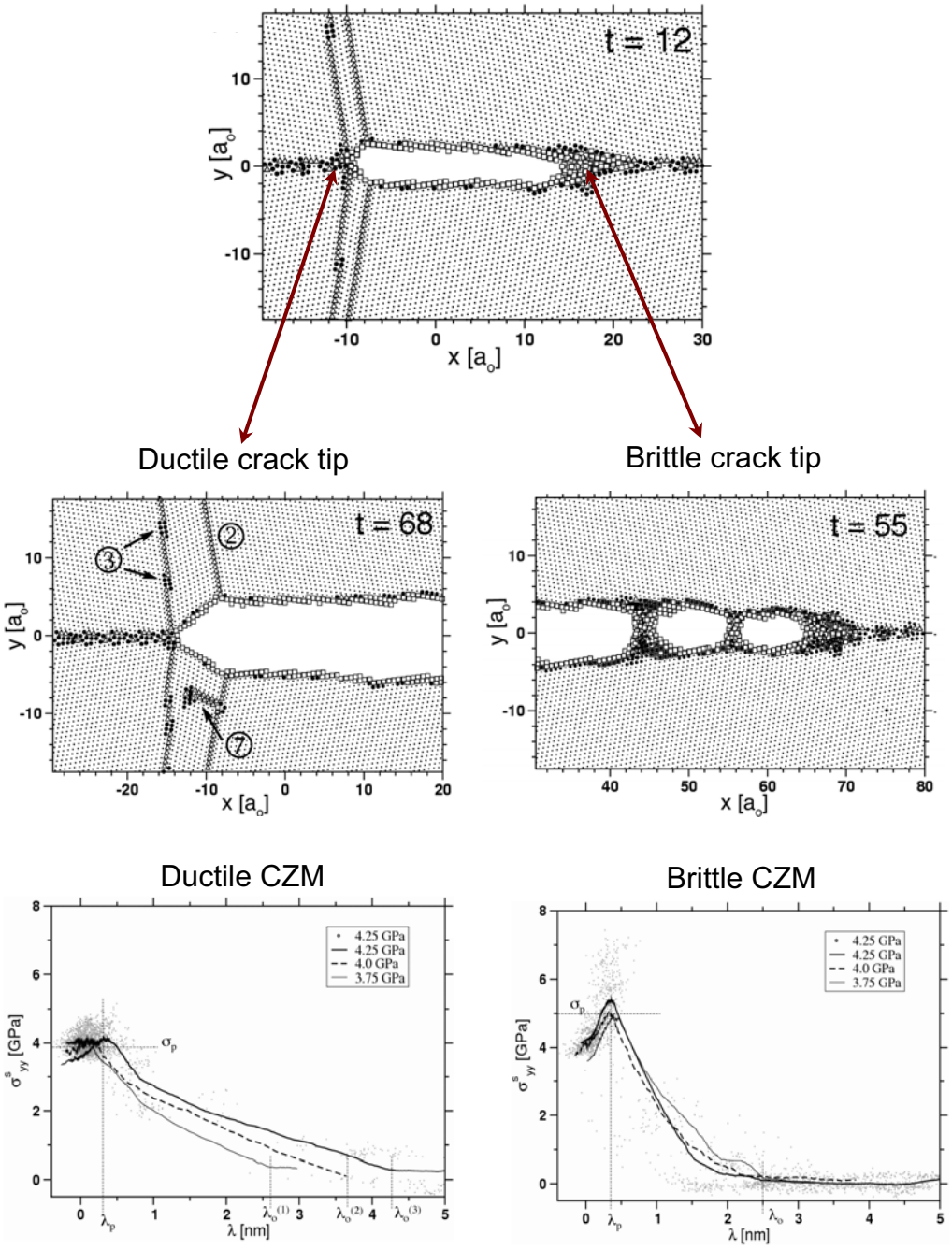

Figure 6. Direction-dependant crack growth behavior incorporated into decohesion finite element formulations (From Yamakov et al., 2006).

The brittle and ductile response of the crack tips shown in Figure 6 is a function of several parameters that include the atomic configuration (e.g. the orientation of slip planes on either side of the grain boundary), and the magnitude of applied external loads.

Figure 7 shows a configuration of a crack plane and slip plane with the angle between the two specified by θ. The orientation of the Burgers vector, ***b***, lying in the slip plane, showing the direction of slip is given by the angle ϕ. For a slip direction aligned with the crack opening such that $\phi = 0$, the Rice criterion (Rice, 1992) for dislocation emission associated with Mode I opening along two propagation directions can be written as

$$\alpha = \frac{\gamma_{us}}{2\gamma_s - \gamma_{GB}} - \frac{(1 \pm \cos\theta)\sin^2\theta}{8} \quad \text{where} \quad \begin{array}{l} \alpha \geq 0 \text{ for brittle fracture} \\ \alpha < 0 \text{ for ductile fracture} \end{array} \tag{8}$$

where $+\cos\theta$ is associated with the -*x* direction and $\cos(\pi - \theta) = -\cos\theta$ is associated with the +*x* direction, and α is the numerical value of the criterion used to predict brittle or ductile fracture depending on its sign. For a Σ99 symmetric tilt GB in aluminum, Yamakov et al. (2006) identifies an unstable stacking-fault energy of γ_{us} = 0.168 J/m^2, a

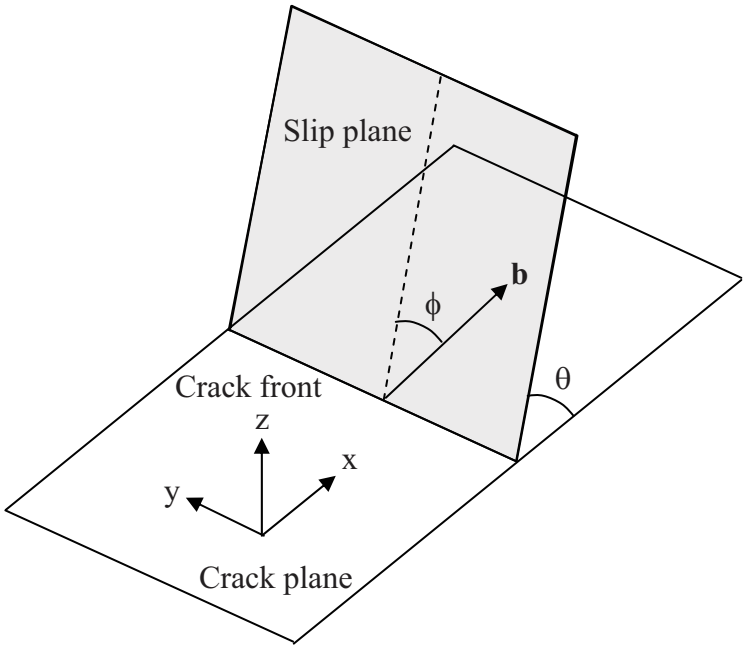

Figure 7. Geometric configuration of a crack with an intersecting slip plane.

surface energy of the GB as γ_s = 0.952 ± 0.010 J/m^2, and an excess GB energy given by γ_{GB} = 0.60 ± 0.05 J/m^2. Substituting in the energy quantities and multiplying through by the denominator in the second term of Equation (8) (because only the sign of α is important), the resulting Rice criterion for this system can be expressed as

$$\alpha = 1.0307 \pm 0.01 - \left(1 \pm \cos\theta\right)\sin^2\theta\,. \tag{9}$$

3. Decohesion Finite Elements

Decohesion finite elements (also referred to in the literature as "interface elements", "cohesive elements," or "CZM elements") were initially introduced by Hilleborg et al. (1976) to study fracture in concrete. Needleman (1987, 1990a, 1990b) later formulated a decohesion element to study dynamic fracture in isotropic solids. The formulations of the elements presented here are based on the work of Beer (1985). The basic topology of decohesion elements is formed by separable surfaces that can open according to constitutive relationships that relate tractions and displacements. The element formulations have found broad application for modeling brittle and ductile fracture whether or not crack paths are known a priori.

When the location of fracture is not known a priori, decohesion elements can be placed between all continuum elements within a finite element mesh. While decohesion elements can add artificial compliance to the model (Diehl, 2008), more complex simulations using adaptive meshing can limit the number of decohesion elements by placing these elements only in regions of high stress (Zhang et al., 2007). Figure 8 depicts a micromechanical simulation of intergranular fracture with decohesion elements placed along all grain boundaries.

The formulation of decohesion finite elements is based on the dimensionality, order of element interpolants, and the particular choice of CZMs that are incorporated into the formulation. Decohesion elements are formulated with two sets of initially coincident

nodes defining two superposed surfaces forming a cohesive interface. In Figure 9, Ω^o represents the middle surface of the element, and Ω^+ and Ω^- represent the top and bottom surfaces of the element after separation. The particular configuration depicted in Figure 9 represents an 8-node linear decohesion element used to simulate the cohesive behavior between connected 8-node solid continuum elements. Shape functions appropriate to the order of assumed variation over the element domain govern the interpolation of quantities over the superposed surfaces.

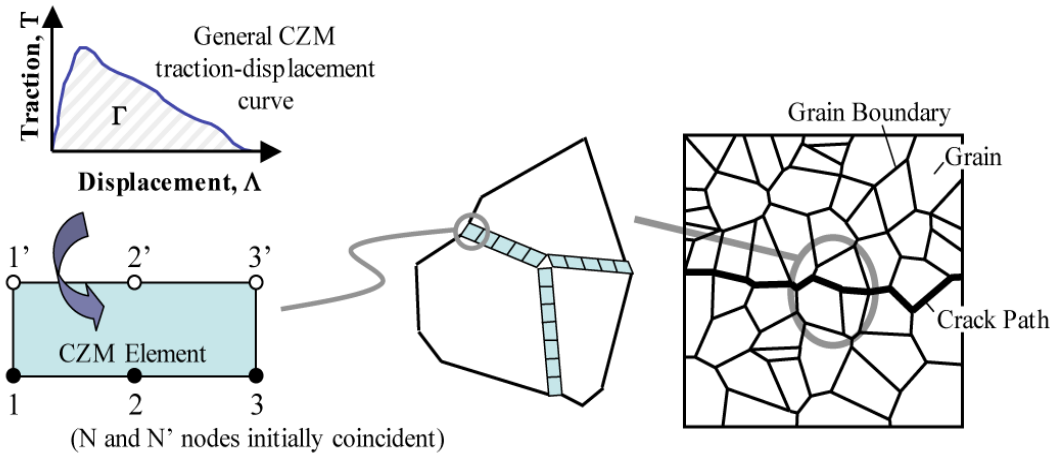

Figure 8. Embedding decohesion elements along GBs to study microstructural fracture.

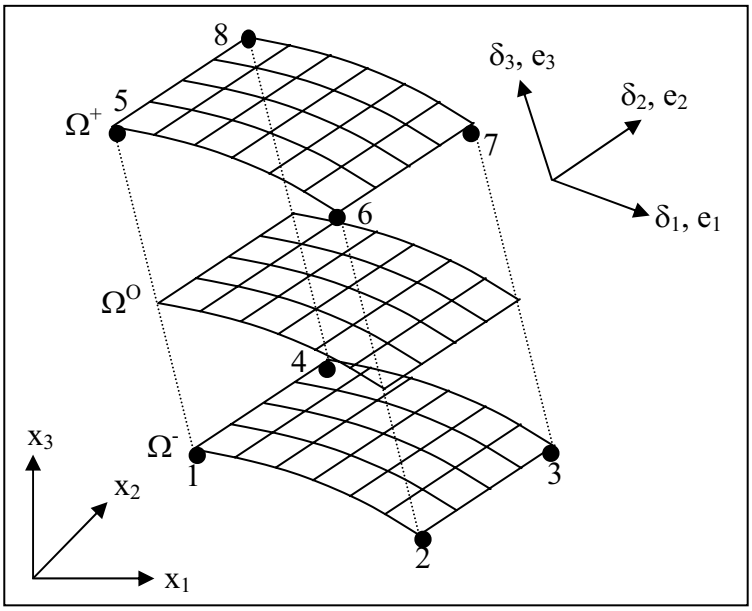

Figure 9. Decohesion element cohesive surfaces.

Fundamental to the response of decohesion elements is the form of the assumed cohesive zone models (CZMs) that govern the prediction of separation – fracture – of element surfaces (Rabinovitch, 2008). As discussed in Section 2, CZMs are defined by displacement jumps, denoted by Δ_i, which measure the discontinuity of the i^{th} displacement components between initially coincident top (δ_i^+) and bottom points on the surfaces (δ_i^-). Thus, the resulting finite element is initially of zero thickness across the assumed fracture plane (see Beer, 1985; Camanho et al., 2003; and Cook et al., 2001). Discretizing each surface into k finite element nodes and assuming that the displacement field varies over the surface defined by standard Lagrangian shape functions N_k yields the relationship

$$\begin{Bmatrix} \Delta_1 \\ \Delta_2 \\ \Delta_3 \end{Bmatrix} = \begin{Bmatrix} \delta_1^+ - \delta_1^- \\ \delta_2^+ - \delta_2^- \\ \delta_3^+ - \delta_3^- \end{Bmatrix} = \begin{Bmatrix} \mathrm{N_k}\delta_{1\mathrm{k}} \\ \mathrm{N_k}\delta_{2\mathrm{k}} \\ \mathrm{N_k}\delta_{3\mathrm{k}} \end{Bmatrix} \tag{10}$$

where δ_{ik} is the i^{th} relative displacement at the k^{th} node referenced to the middle surface of the element Ω^O. Transforming between local (e_1,e_2,e_3) and global (x_1,x_2,x_3) coordinate systems using the transformation tensor T_{ij} yields

$$\{\mathrm{u}\} = [\mathrm{T}]\{\Delta\} = [\mathrm{T}][\mathrm{N}]\{\delta\} = [\mathrm{B}]\{\delta\} \tag{11}$$

Relating the element tractions, τ_i, to the relative element displacements, u_i, is performed using the decohesion element constitutive operator, D_{ij}, as

$$\{\tau\} = [\mathrm{D}]\{\mathrm{u}\} \tag{12}$$

The governing equation can be obtained from the principle of virtual work

$$\int_{\Omega^{\mathrm{o}}} \mathrm{d}\{\mathrm{u}\}^{\mathrm{T}} \{\tau\} \mathrm{d}\Omega^{\mathrm{o}} - \{\mathrm{f}\}^{\mathrm{T}} \mathrm{d}\{\mathrm{u}\} = 0 \tag{13}$$

which yields, for a geometrically linear problem, the relationship

$$\int_{\Omega^o} [B]^T \{\tau\} d\Omega^o - \{f\}^T = 0 \tag{14}$$

where [*B*] is constant. Substituting Equations (11) and (12) into Equation (14) yields the standard governing equation for linear elastostatics

$$[\mathrm{K}]\{\delta\} = \{\mathrm{f}\} \tag{15}$$

where

$$[\mathrm{K}] = \int_{\Omega^o} [\mathrm{B}]^T [\mathrm{D}][\mathrm{B}] d\Omega^o \tag{16}$$

The constitutive matrix, [*D*], is formulated based on the assumed traction-displacement relationship.

Different features can be incorporated into the element formulation. For example, Turon et al. (2004) utilizes a tangent constitutive relation based on bilinear CZMs that incorporates a damage parameter as a state variable for mixed-mode failure and a variable term that accounts for interpenetration due to possible closing in Mode I fracture. Various additional details of decohesion element formulations can be found in Chen et al., 1999; Foulk et al., 2000; Alfano and Crisfield, 2001; Goyal et al., 2002; Camanho et al., 2003; Segurado and Llorca, 2004; Gustafson et al., 2008; Hamitouche et al., 2008; and Van den Bosch et al., 2007. However, most of the differences in these formulations pertain to specific definitions of CZM relationships incorporated into the decohesion element.

An additional issue relevant to the development of CZMs regards the initial stiffness associated with the constitutive relationship for each fracture mode. For macroscopic analysis, this initial stiffness assumes the role of a penalty constraint. A formal penalty parameter would assume the highest value that would not cause ill-conditioning in the

global element stiffness matrix. However, in practice, this constraint is set to a high value to minimize the relative displacements between the top and bottom surfaces before the onset of softening, but does allow numerically small displacements to be calculated that are compared with the onset relative displacement at which softening begins. This onset displacement, denoted by Δ_o in Figure 4, is equal to the peak traction divided by the selected penalty stiffness and is, thus, a small quantity. However, a consequence of this is the introduction of a spurious compliance into the model that can alter results, particularly in models where decohesion elements are placed between many continuum elements. However, at nanoscopic length scales, this initial stiffness is typically calculated based on the elastic properties of the grain boundary or between lattice planes because the thickness of the cohesive surface can no longer be generally regarded as infinitesimal. In this case, the initial stiffness of the CZM no longer approximates a mathematical penalty parameter but is reduced to represent the actual stiffness of a finite thickness cohesive zone. Under arbitrarily small loads, the displacement field is not homogeneous, and the cohesive surface exhibits an elastic separation due to straining below the peak traction. To avoid adding spurious compliance to the model due to a numerically finite initial stiffness, either an initial thickness may be assigned to the decohesion elements or the elastic properties of adjacent continuum elements may be adjusted.

Convergence difficulties have been encountered and have been related to numerical problems caused by abrupt changes in the slope of the CZM relationship – such as at the vertices of triangular and trapezoidal CZM relations - during loading and unloading cycles in which large variations can occur in computing the tangent stiffness matrix (Gao and Bower, 2004). Another effect that can hinder convergence involves the type of numerical quadrature used to evaluate the element integrals. It has been found that Gaussian quadrature tends to couple kinematic degrees of freedom across the element that can be seen in the eigenmodes of the element deformation states. Conversely, Newton-Cotes quadrature methods act to uncouple the eigenmodes and have been associated with an improvement in convergence behavior (Schellekens and de Borst, 1993). Additional numerical aspects, such as bounds on element size, have been

presented (Allen and Searcy, 2000; Tomar et al., 2004; and Turon et al., 2007), and augmented solution schemes that include numerical relaxation to improve convergence characteristics have been advanced (Gao and Bower, 2004).

3.1 Directional Decohesion Element Formulation

The directional dependence of Mode I fracture presented in Section 2.1 motivated the development of a directional decohesion finite element formulation for simulating intergranular crack propagation. The unique feature of this element is the adaptive application of different CZMs depending on the grain orientation and the internal computation of the direction of Mode I propagation. This element incorporates the direction-dependant CZMs for Mode I opening and utilizes a single Mode II and Mode III CZM for computing an effective mixed-mode CZM as explained in Section 2.0. The appropriate brittle or ductile Mode I CZM is selected based on Rice's criterion that accounts for the orientation of the surrounding slip systems in the direction of propagation (see Figure 6). Both 1-D and 2-D element configurations are presented which incorporate Rice's criterion (Rice, 1992) to apply the appropriate CZM during an incremental-iterative solution procedure. The directional decohesion element formulations have been encoded into user-defined element (UEL) subroutines to enable simulations to be performed using the commercial finite element code ABAQUS®[1]/Standard (2008).

Until the final effective opening displacement has been reached and the decohesion element stiffness terms are zero, calculations are performed using the relative u, v, and w nodal displacements to approximate the displacement gradients over the element surface and determine the direction of propagation. For cases in which various opening displacements are equal or zero, a default direction is assumed. A propagation vector, $\vec{\boldsymbol{d}}$, is used to specify the direction of Mode I fracture as is required in the application of Rice's criterion. A second propagation vector, $\vec{\boldsymbol{s}}$, gives the direction of relative tangential

[1] ABAQUS® is manufactured by Dassault Systèmes Simulia Corp. (DSS), Providence, RI, USA

motion of the cohesive surfaces. At microscopic length scales where the behavior of discrete atoms and slip planes are significant, there is a distinction between Mode II and Mode III sliding and fracture. Fracture by definition generates new free surface area, while sliding involves bond breakage which reform between the upper and lower surfaces. The determination of relative amounts of tangential sliding and fracture is an issue that is currently unresolved and will not be elaborated here; a further discussion can be found in Saether (2008).

The directional decohesion elements developed in the current work consist of a 1-D 6-node decohesion element for joining 2-D quadratic triangular continuum elements and a 2-D 12-node decohesion element for joining 3-D quadratic tetrahedral elements. For both elements, the orientation of slip planes with respect to the cohesive surface is required input. To apply Rice's criterion, the direction of Mode I opening for each decohesion element must be determined.

For the 1-D decohesion element, the direction of opening or sliding is simply given by the sign of the slope of the relative normal displacements or relative tangential displacements along the element. Figure 10 shows the 6-node decohesion element configuration. Although the element is quadratic, the Mode I opening direction is determined by computing an approximate linear gradient of the relative opening displacements, Δv_i, over the element using only the end nodes. The degree of sliding in Mode II is computed by a summation of all relative x-displacements, Δu_i, over the element.

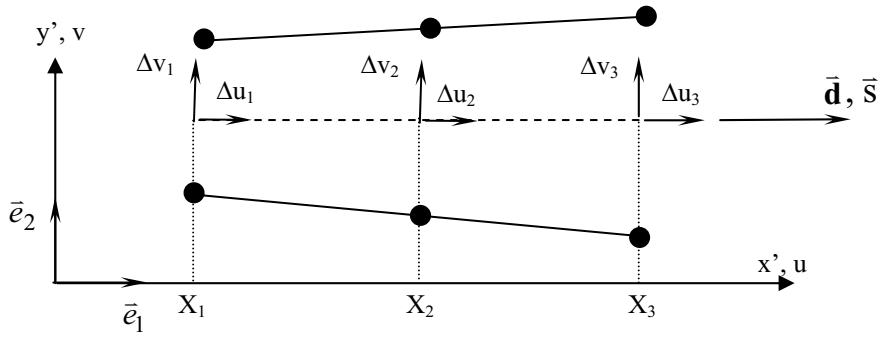

Figure 10. Relative opening displacements for Mode I and Mode II fracture in a 6-node quadratic decohesion element.

The kinematics and integration scheme used in the new 6-node 1-D directional decohesion element is similar to the element presented by Alfano and Crisfield (2001). The sign of the difference between relative displacements determines the directionality of Mode I opening and Mode II sliding across the element. In determining the sense of relative motion, only the end nodes of the upper or lower surface need to be considered. The propagation vectors are then computed as

$$\vec{d} = \mathrm{Sgn}\left(\Delta v_3 - \Delta v_1\right)\vec{e}_1 \tag{17}$$

$$\vec{s} = \mathrm{Sgn}\left(\Delta u_1 + \Delta u_3\right)\vec{e}_1 \tag{18}$$

where *Sgn* indicates the Sign function.

For the 2-D 12-node decohesion element shown in Figure 11, the surface may be defined by the local mapped *x'* and *y'* coordinates corresponding to the node positions, and can be defined using a general scalar field representation as $\phi = F(x',y')$, where ϕ represents the variation of a relative displacement component over this region. Using this surface, the components of the propagation vectors can be expressed in terms of the element *x'* and *y'* coordinates. The equation of a surface is given by

$$Ax' + By' + Cz' = D \tag{19}$$

where *x*' and *y*' are the mapped coordinate axes, and *z*' is the value of the scalar field at each (*x*',*y*') point over the domain. The normal to this surface is given by

$$\vec{n} = A\vec{e}_{x'} + B\vec{e}_{y'} + C\vec{e}_{z'} \tag{20}$$

where $\vec{e}_\alpha$ are unit basis vectors in the local element coordinate system, and the components of interest are calculated as

$$A = \begin{vmatrix} 1 & y_1' & \phi_1 \\ 1 & y_2' & \phi_2 \\ 1 & y_3' & \phi_3 \end{vmatrix} = y_1'(\phi_2 - \phi_3) + y_2'(\phi_3 - \phi_1) + y_3'(\phi_1 - \phi_2) \tag{21}$$

$$B = \begin{vmatrix} x_1' & 1 & \phi_1 \\ x_2' & 1 & \phi_2 \\ x_3' & 1 & \phi_3 \end{vmatrix} = \phi_1(x_2' - x_3') + \phi_2(x_3' - x_1') + \phi_3(x_1' - x_2').$$

All global displacement quantities are mapped to a local element coordinate system for the determination of opening behavior. Failure propagation vectors are computed in the local frame and mapped back to the global coordinate system to compare with grain orientation angles to select which CZM law is to be applied.

The 12-node decohesion element shown in Figure 11 is defined with respect to a local (x',y',z') element coordinate system, and the kinematics are similar to an element presented by Segurado and Llorca (2004).

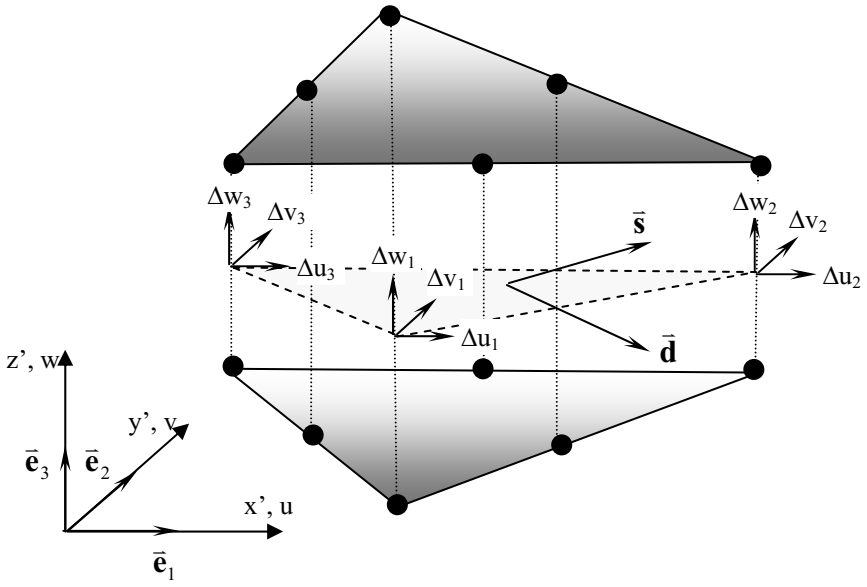

Figure 11. Estimated direction of GB opening and sliding in mixed-mode fracture.

For Mode I, the expected opening direction is given by the propagation vector, $\vec{d}$, as

$$\vec{\mathrm{d}}_{\mathrm{opening}} = \mathrm{A}_{\mathrm{I}}\,\vec{\mathrm{e}}_1 + \mathrm{B}_{\mathrm{I}}\,\vec{\mathrm{e}}_2 \tag{22}$$

where the A_I and B_I are given in Equations (21) with $\phi_i = \Delta w_i$. Because the current development assumes a symmetric tilt GB, the orientation angle θ specifies the relative angle between a slip plane and the cohesive zone crack plane. The direction of opening in Mode I is given by $\beta = \tan^{-1} B_I / A_I$.

This element can be enhanced to include a full description of grain boundary orientation with respect to surrounding slip planes. For the present analysis, it is assumed that the crack surface is offset from the nearest slip plane by a single tilt angle, θ, as shown in Figure 9. Thus, defining a local coordinate system, (x',y'), aligned with the GB, the direction of opening is simply given by the sign of the A_I component of the propagation vector $\vec{d}$ where Sgn(A_I) < 0 and Sgn(A_I) > 0 indicates opening in the $-x$ and $+x$ directions, respectively.

The component directions of Mode II and Mode III fracture are given by Equations (21) with $\phi_i = \Delta u_i$ and $\phi_i = \Delta v_i$, respectively. The propagation vectors for these two modes are given by

$$\begin{aligned} \vec{\mathrm{s}}_{\Delta \mathrm{u}} &= \mathrm{A}_{\mathrm{II}}\,\vec{\mathrm{e}}_1 + \mathrm{B}_{\mathrm{II}}\,\vec{\mathrm{e}}_2 \\ \vec{\mathrm{s}}_{\Delta \mathrm{v}} &= \mathrm{A}_{\mathrm{III}}\,\vec{\mathrm{e}}_1 + \mathrm{B}_{\mathrm{III}}\,\vec{\mathrm{e}}_2 \end{aligned} \tag{23}$$

The direction of the in-plane propagation vectors may then be used to quantitatively determine the degree of mode mixity for fracture tangential to the crack plane. Directional dependence of Mode II and Mode III fracture at atomistic length scales have yet to be developed, however, once defined with suitable selection criteria, these may be included into the element formulation in an identical manner as with the automated selection of appropriate Mode I CZMs.

4.0 Simulation of Fracture in 2-D and 3-D Aluminum Polycrystals

Investigations of fracture in 2-D and 3-D aluminum polycrystals have been performed. One study involves a 2-D polycrystal model in which CZM parameters describing brittle and ductile intergranular fracture propagation are varied to simulate the effect of different GB fracture behavior. This simulation does not include directionality of fracture but is instead focused on the effect of CZM parameterization on the overall stress-strain behavior of the model and final fracture path. Another study examines two 3-D polycrystal models to assess the effectiveness of directional decohesion finite elements that automatically select a brittle or ductile CZM using Rice's criterion based on GB orientation with respect to adjacent slip planes and the opening direction of Mode I fracture.

4.1 Study of CZM Parameter Variation on Fracture Development in a 2-D Polycrystal

Figure 12 shows a tessellated 2-D polycrystalline microstructure having many grain boundaries. The model has dimensions of $l_x = l_y = 47.5$ nm, and consists of 50 grains. Six-node triangular finite elements are used to represent the elastic continuum having the elastic properties of aluminum (E=72 GPa, ν=0.34). Parametric studies were performed by linearly combining the CZM parameters using the MD extracted cohesive zone curves describing brittle and ductile Mode I fracture shown in Figure 8 (Glaessgen et al., 2006). The polycrystalline microstructure is simulated under a uniform tensile strain U_y loaded incrementally to 22% strain. CZM properties for shear sliding under

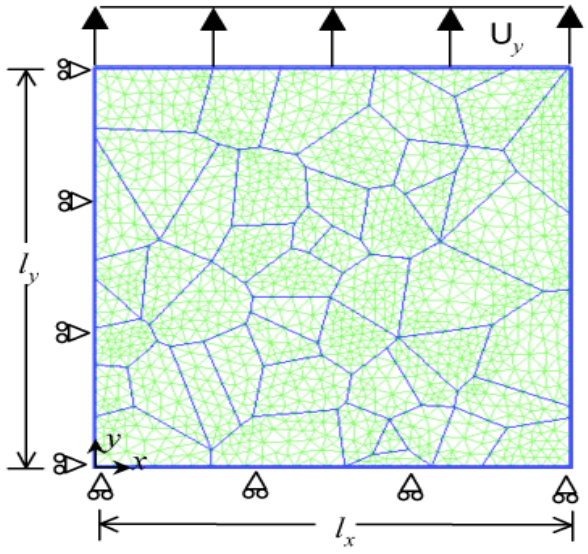

Figure 12. Idealized microstructural model.

Mode II loading were arbitrarily selected to simulate an elastic-perfectly plastic behavior. All parameters are shown in Table 2.

Using brittle Mode I CZM properties for all the GBs, Figure 13 shows the sequence of decohesion processes under normal applied displacements. The CZM parameters for Mode I opening obtained from MD analysis yielded an initial GB stiffness that is similar to the stiffness of the adjoining grains, and thus does not act as a numerical penalty constraint. Therefore, these interfaces begin to exhibit relative displacement at load levels below the peak traction in the elastic region of the bilinear CZM. This is depicted in Figure 13a where no magnification has been applied to the relative displacements of the cohesive zones along the GBs and the black regions indicate significant relative displacements along the grain interfaces prior to full opening of the CZMs. At higher applied strains, the lowest energy associated with GB opening dictates the location at which a dominant microcrack begins to form (Figure 13b). At a critical applied strain, the local coalescence of GB opening forms a dominant microcrack as shown in Figure 13c. It is also seen that due to unloading after the dominant microcrack has fractured the model, the stiffness in other decohesion elements acts to pull the opening cohesive zones back to an unloaded state.

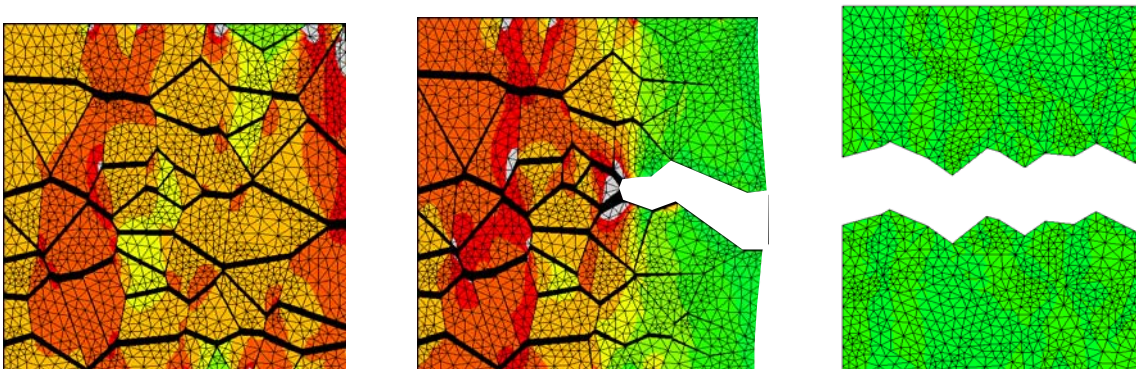

(a) Initial opening of GBs, $\varepsilon_v = 16\%$

(b) Local crack formation, $\varepsilon_v = 17\%$

(c) Dominant microcrack, $\varepsilon_v = 22\%$

Figure 13. Dominant microcrack formation in a polycrystal model using cohesive zone models.

Prior to demonstrating the behavior of directional decohesion elements, the qualitative influence of CZM parameters will be illustrated through comparative simulations in which properties for Mode I fracture are assigned as a parametric series of proportions of the Mode I brittle and ductile CZM parameters presented in Table 3. These parameters, ϕ, were obtained as

$$\phi_{combined} = \alpha\, \phi_{brittle} + (1 - \alpha)\, \phi_{ductile} \tag{24}$$

where α ranged from 1.0 to 0.0. The Mode II shear parameters were arbitrarily selected to simulate an elastic-perfectly plastic behavior. The values chosen were τ^o_{mx} = 0.8 GPa and Δ^c_{mx} = 100 nm which were kept constant in all simulations. Material properties for the grains were assumed as linear isotropic with a Young's modulus of 100.0 GPa and Poisson's ratio of 0.34.

Table 2. CZM parameters defining Mode I behavior at the 2-D crack tip.

CZM	Brittle Mode I	Ductile Mode I
τ^o_{mx} (GPa)	5.00	3.95
Δ^o (nm)	1.07	0.85
Δ^c_{mx} (nm)	2.17	5.65
G (J/m^2)	5.43	11.2

Table 3. CZM parameters used to simulate different proportions of elastic and plastic Mode I opening behavior at the 2-D crack tip.

Mode I CZM parameters.

CZM	α	Δ^c_{mx} (nm)	G (J/m^2)
C1	1.00	2.17	5.43
C2	0.75	3.04	7.20
C3	0.50	3.91	8.75
C4	0.25	4.78	10.1
C5	0.00	5.65	11.2

Figure 14 shows the resulting stress-strain response of the polycrystal model using variations in the proportion of brittle and ductile Mode I cohesive zone behavior. The global stress versus strain results demonstrate the imposed trend of decreasing maximum

stress with increasing ductility in the CZM law. Because the relative tangential sliding motion in shear is assumed to be independent of Mode I separation, all the parameterized models follow a similar extended softening response that continues until ultimate failure. Due to the different parameters used to define Mode I cohesive properties of the GBs, three different crack paths where exhibited by the models and are shown in Figure 14.

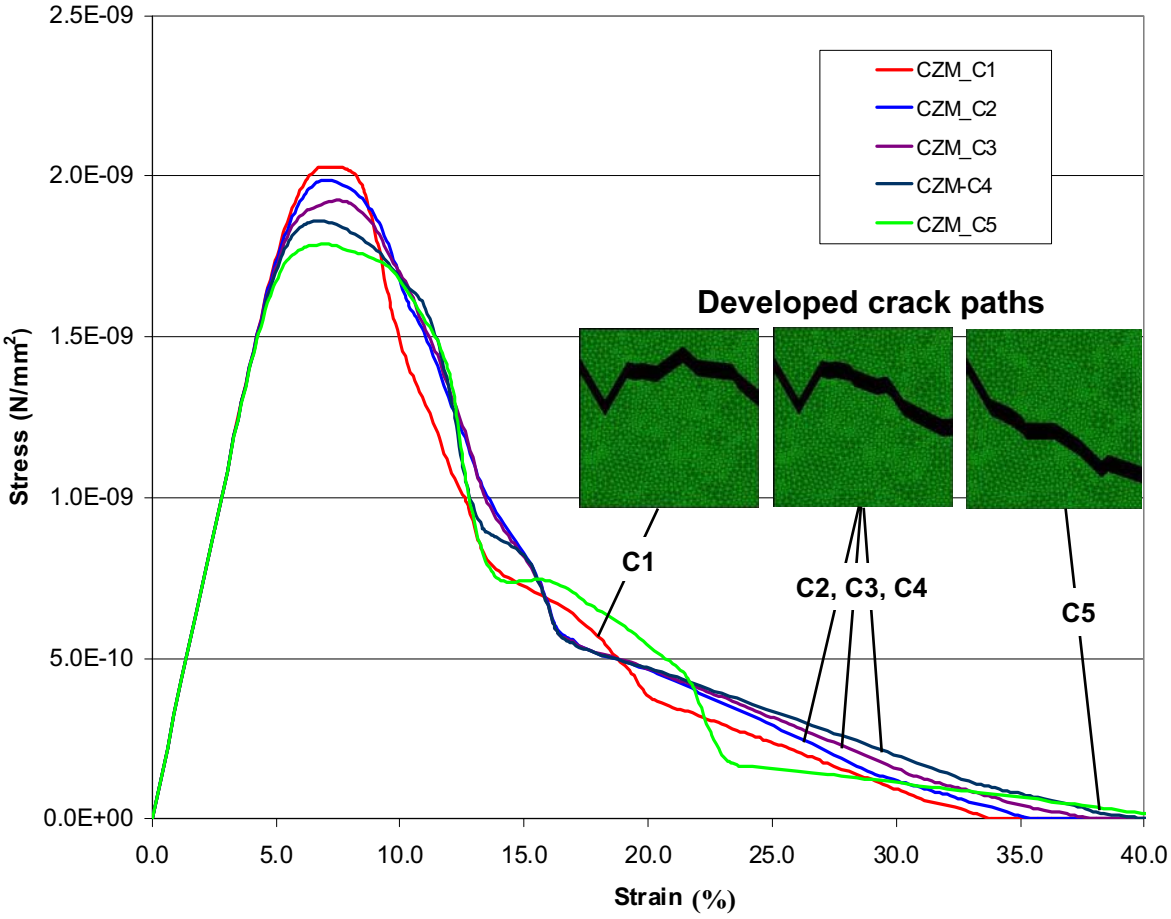

Figure 14. Parametric study of Mode I stress/strain response in a polycrystal with brittle vs ductile GBs.

4.2 Study of Directional Decohesion Elements on Fracture Development in 3-D Polycrystals

Two 3-D polycrystal models have been developed to illustrate the influence of CZM parameters and the functionality of directional decohesion elements that account for grain

orientation and Mode I fracture opening direction. The first model focuses on the preferred propagation of fracture along GBs forming a junction between multiple grains. In a 3-D model, grain boundaries typically form triple lines and quadripole junctions. However, to best illustrate the directional behavior of fracture propagation, the model is limited to 3 grains forming a triple junction. Modeling the cohesive surfaces placed along each GB using the 12-node directional decohesion element discussed in Section 3.1 will, in general, require five independent angles to fully define the orientation of a flat GB in a defect-free material and the availability of accurate CZMs to describe directional fracture characteristics. This information will be required as input to each decohesion element defining a particular GB. However, because of the limited characterization of GB fracture behavior, for the present analysis, each GB is assumed as a symmetric tilt GB that can be characterized by a single misorientation angle. In order to apply Rice's criterion, the local direction of opening must be computed and the angle, θ, between the opening direction and the local slip plane orientation must be determined.

The grains are assumed to be isotropic and linear elastic (E = 100 GPa, $\nu = 0.3$), and the CZM parameters used in this simulation are presented in Table 4. The directional decohesion element detailed in Section 3.1 was coded into a user-defined element for use in ABAQUS. This element routine implemented Rice's criterion which was automatically applied during the simulation to determine whether brittle or ductile Mode I CZM parameters were to be applied. The model geometry, loading, and results of changing the tilt angle for each GB is shown in Figure 15.

Table 4. CZM parameters defining GB properties in the triple junction model.

CZM	Brittle Mode I	Ductile Mode I	Shear
τ^o_{mx} (GPa)	5.00	8.00	0.80
Δ^o (nm)	1.07	1.71	0.40
Δ^c_{mx} (nm)	2.17	8.00	1.00

As shown in Figure 15, simulation of a 3-D grain junction under a constant biaxial load state shows that different fracture paths are predicted using the formulated directional decohesion element by changing the tilt angle associated with each GB.

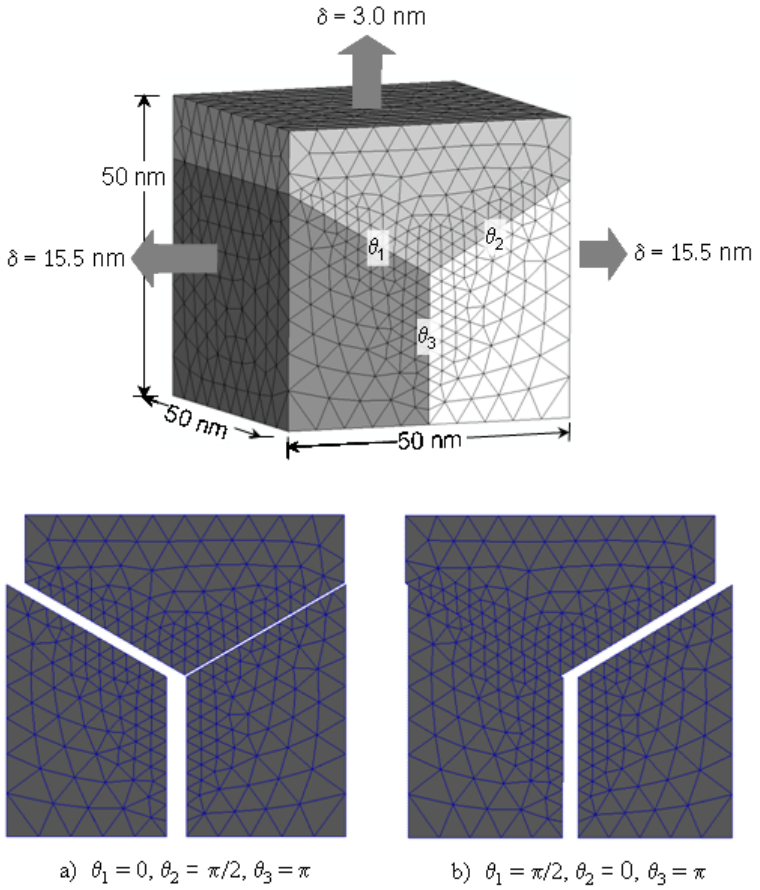

Figure 15. Simulation of a triple junction showing different opening behavior with different assumed GB tilt angles using directional decohesion elements.

The second model is a 3-D polycrystal model that is used to illustrate the effect of changing CZM parameters associated with GBs on the global stress-strain response and fracture surface creation. This model was constructed by extruding the 2-D model used in Section 4.1 in the thickness (*z*-) direction and is depicted in Figure 16. The same loading and boundary conditions shown in Figure 12 were used, however, to fix the model against motion in the thickness direction, roller supports were placed on the $z = 0$ surface of the model. The model incorporates directional decohesion elements along each GB and assigns an initial random material orientation for each grain. CZM parameters are systematically varied to simulate the fracture behavior of other types of symmetric tilt GBs.

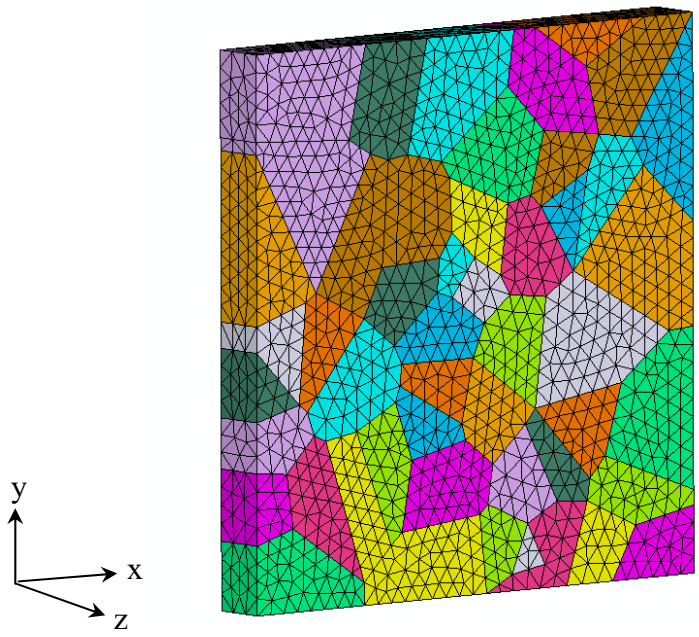

Figure 16. Model of a 3-D 50-grain microstructure.

To simplify the geometry of the model, each grain was assumed to have a principal slip system normal to the global *x*-*y* coordinate system. Thus, grain orientation of the n^{th} grain can be assigned using a single angle, β_n, ranging from $(-\pi,+\pi)$ and defined with respect to the *x*-axis as shown in Figure 17.

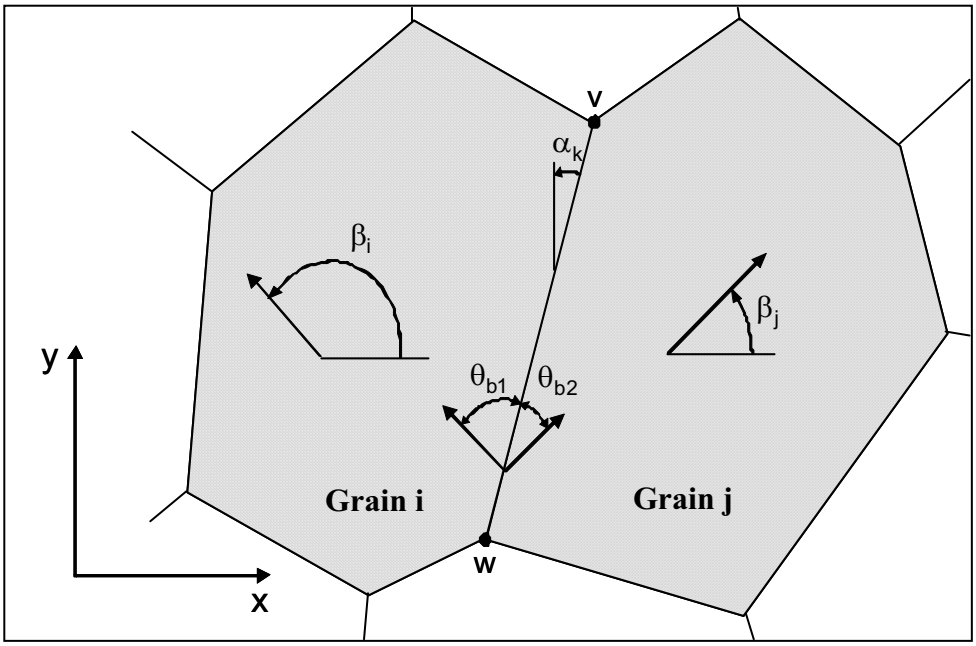

Figure 17. Geometric description of grain orientation and grain boundaries.

For a simple tilt grain geometry, the grain boundary orientation is defined by the angle, α_k, which is measured counterclockwise to the global *y*-axis. This angle is computed as

$$\alpha_k = \mathrm{Tan}^{-1}\left(\frac{v_x - w_x}{v_y - w_y}\right) \tag{25}$$

where *v* and *w* denote vertex positions defining the ends of the GB. It follows that the tilt angles, θ_{b1} and θ_{b2}, of the GB with respect to the grain slip system are given by

$$\begin{aligned} \theta_{b1} &= \beta_i - \pi/2 + \alpha_k \\ \theta_{b2} &= \pi/2 - \beta_j - \alpha_k \end{aligned} \tag{26}$$

A further simplification is required to allow the parameterized MD results for a symmetric tilt grain boundary to be used. Therefore, each tilt angle is replaced by an average value, $\overline{\theta}$, obtained as

$$\overline{\theta} = \left(\theta_{b1} + \theta_{b2}\right)/2 = \left(\beta_i - \beta_j\right)/2 \tag{27}$$

The 3-D 25-grain microstructure model, shown in Figure 16, has *x* and *y* dimensions of 47.5 nm and a thickness of 4.75 nm. The grain properties were modeled as linear isotropic with a modulus of 100 GPa and a Poisson's ratio of 0.34. Although similar geometry and grain properties where used for the 2-D and 3-D polycrystal models, CZM parameters were not made to coincide because these parameters were used differently in the two models to generate effective properties for the decohesion elements in the two models that precludes a direct comparison of deformation response. The Mode I CZM parameters used τ_{mx}^{o} = 5 GPa for brittle fracture and τ_{mx}^{o} = 4 GPa for ductile fracture in the current simulation. Both CZMs used an initial stiffness of 4.69 GPa. For Mode II and Mode III deformation fields, the maximum traction was held constant at 0.8 GPa, and the maximum opening displacement was held constant at 2.0 nm. The varied CZM

parameters used to represent other GB configurations with differing degrees of elastic and plastic response are presented in Table 5. These parameters were derived from CZM properties calculated by Yamakov et al. (2006) for a symmetric tilt Σ99 GB in aluminum.

Table 5. CZM parameters used to simulate different proportions of elastic and plastic Mode I opening behavior at the 3-D crack tip.

Brittle Mode I CZM. Peak traction held constant at τ^{o}_{mx} = 5.0 GPa.

CZM	Δ^{c}_{mx} (nm)	G (J/m^2)
D1	2.17	5.42
D2	2.89	7.22
D3	4.33	10.84
D4	6.50	16.25

Ductile Mode I CZM. Peak traction held constant at τ^{o}_{mx} = 4.0 GPa.

CZM	Δ^{c}_{mx} (nm)	G (J/m^2)
D1	3.75	7.50
D2	5.00	10.0
D3	6.25	12.5
D4	10.0	20.0

Figure 18 shows a representative evolution of a dominant microcrack in the 3-D polycrystal model. As directional decohesion elements along various GBs exhibit softening due to damage accumulation, local load redistribution influences which GBs will ultimately fracture and create part of the dominant microcrack. For simplicity in the CZM formulation and finite element implementation, unloading is assumed to follow a path back to the origin to avoid storing and enforcing as a nodal constraint any evolving inelastic displacements during simulation. Thus, as various regions away from the dominant microcrack are unloaded, the directional decohesion elements along GBs in these regions pull the opening GBs back to a closed state.

The global stress-strain response of the model is shown in Figure 19. For each set of CZM parameters listed in Table 5, the initial random assignment of grain orientation causes the slight difference in the initial elastic stiffness between ductile and brittle CZMs such that each model exhibits a similar global stress-strain response until local softening due to damage accumulation commences at ~9.35% strain. The variation in the maximum ultimate displacement for each model shows the expected increase in the degree of softening with increasing Δ_{mx}^{c} in the nonlinear portion of the global stress-strain curves. The difference in predicted crack paths is due to changes in the internal load transfer due to variations in the Mode I CZM properties of the GBs.

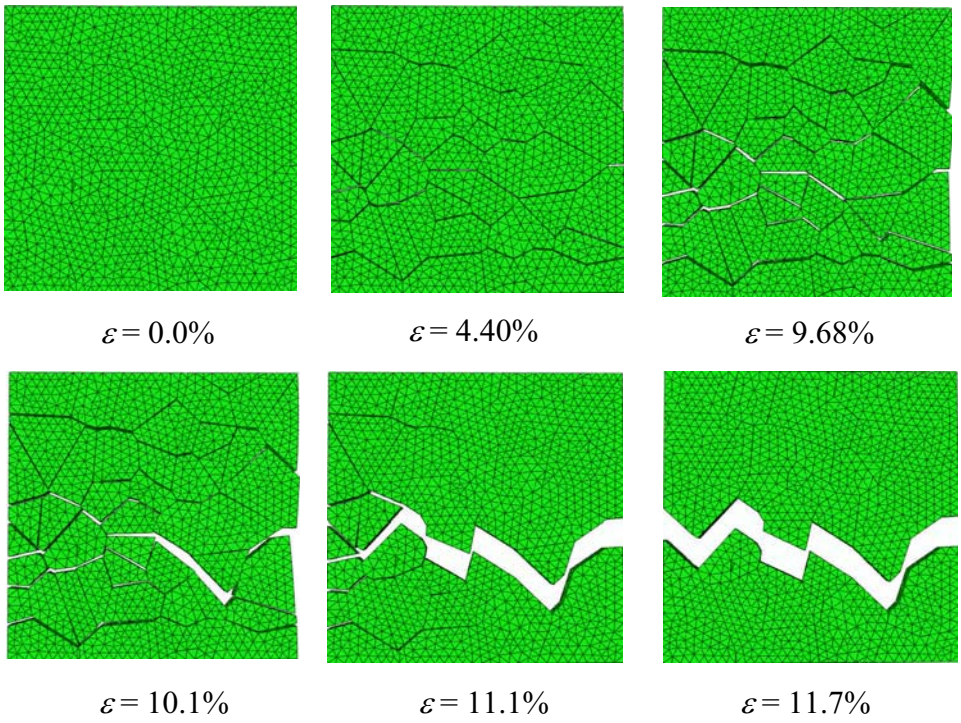

Figure 18. Fracture sequence in the 3-D polycrystal model.

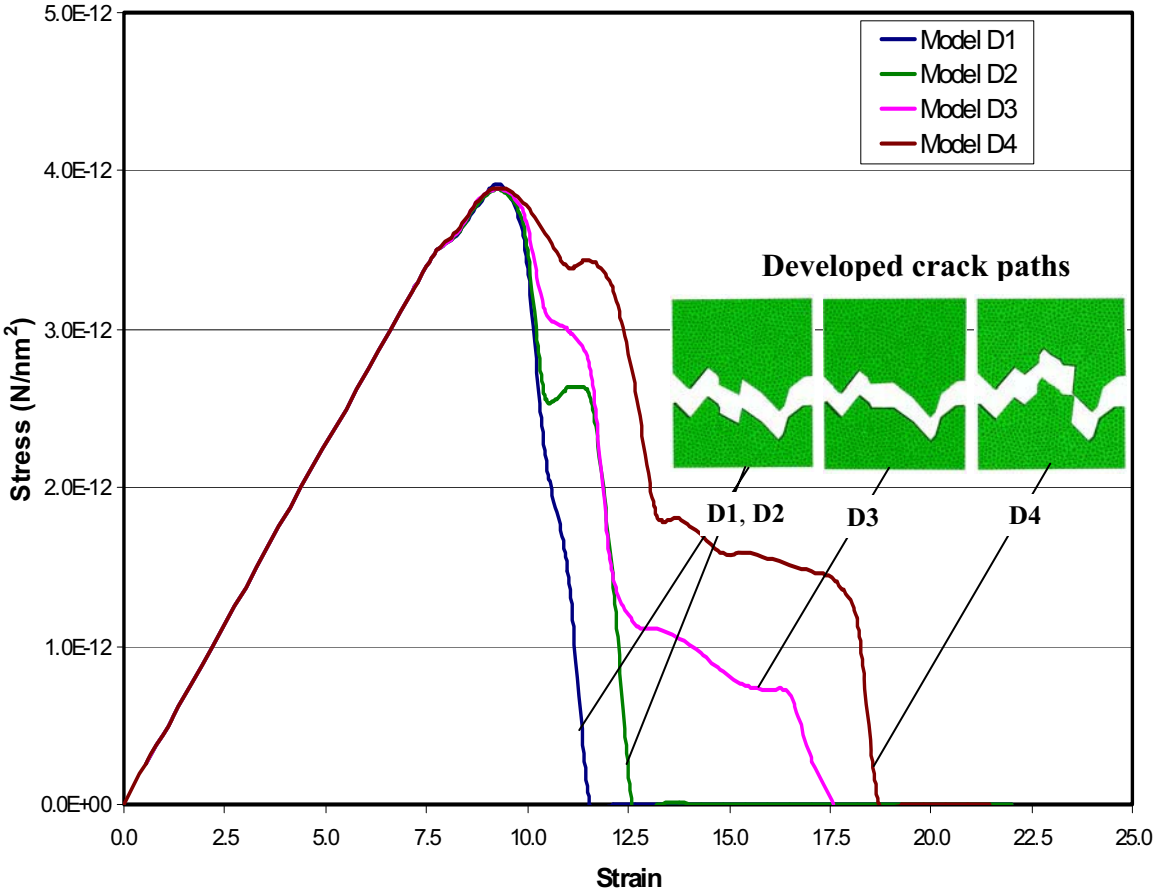

Figure 19. Stress-strain curves for the 3-D polycrystal model.

5. Concluding Remarks

The directional decohesion element developed herein adds an additional feature to decohesion element formulations that allows the element to alter its cohesive behavior during the course of nonlinear finite element analysis. For simulation of microstructural failure within polycrystals, the directional decohesion element incorporates Rice's criterion for dislocation emission to automatically apply an appropriate brittle or ductile CZM. The selected CZM governs intergranular fracture based on surrounding grain orientation and opening direction in various fracture/sliding modes. Two simplistic

illustrative examples of how results from atomistic simulations might be incorporated within the direction decohesion elements were presented.

For arbitrary GB orientations, the directional decohesion element will require additional rotation angles to be input to define the GB and perform more involved calculations of the relative orientation of the cohesive plane and surrounding slip systems. Some additional derivations might be required to modify the opening criterion for the case when the crack plane does not lie along an atomic plane and intersects a slip plane in a skewed orientation. However, the most important requirement for the realistic simulation of failure in metallic polycrystals is the determination of CZMs to quantify GB fracture behavior for the full multi-dimensional space of GB configurational parameters.

6. References

ABAQUS/Standard User's Manual, 2008, Dassault Systèmes Simulia Corp. (DSS), Providence, RI, USA.

Alfano, G., and Crisfield, M.A., 2001, "Finite Element Interface Models for the Delamination Analysis of Laminated Composites: Mechanical and Computational Issues," *Int. J. Num. Meth. Engrg.*, **50**, pp. 1701-1736.

Allen, D.H., and Searcy, C.R., 2000, "Numerical Aspects of a Micromechanical Model of a Cohesive Zone," *J. Reinf. Plast. and Comp.*, **19**, pp. 240-248.

Barenblatt, G.I., 1959, "The Formation of Equilibrium Cracks during Brittle Fracture. General Ideas and Hypothesis. Axially-Symmetric Cracks," *Prikl. Matem. I mekham*, **23**, pp. 434–444.

Barenblatt, G.I., 1962, "Mathematical Theory of Equilibrium Cracks in Brittle Fracture," In: Dryden, H.L., von Karman, T. (Eds.), *Advances in Applied Mechanics, vol. VII*. Academic Press, New York, pp. 55–125.

Beer, G., 1985, "An Isoparametric Joint/Interface Element for the Finite Element Analysis," *Int. J. Numer. Meth. Engrg*., **21**, pp. 585-600.

Benzeggagh, M.L. and Kenane, M., 1996, "Measurement of Mixed-Mode Delamination Fracture Toughnesss of Unidirectional Glass/Epoxy Composites with Mixed-Mode Bending Apparatus," *Comp. Sci. and Tech.*, **49**, pp. 439-439.

Bilby, B.A., and Bullough, R., 1954. "The Formation of Twins by a Moving Crack," *Phil. Mag.*, **45**, pp. 631-646.

Camacho, G.T., and Ortiz, M., 1996, "Computational Modeling of Impact Damage in Brittle Materials," *Int. J. Solids and Struct.*, **33**, pp. 2899–2938.

Camanho, P.P., Davila, C.G., and De Moura, M.F., 2003, "Numerical Simulation of Mixed-Mode progressive Delamination in Composite Materials," *J. Comp. Mat*., **37**, pp. 1415-1438.

Chandra, N., Li, H., Shet, C., and Ghonem, H., 2002, "Some Issues in the Application of Cohesive Zone Models for Metal-Ceramic Interfaces," *Int. J. Solids & Struct.*, **39**, pp. 2827-2855.

Chen, J., Crisfield, M., Kinloch, A.J., Busso, E.P., Matthews, F.L., and Qui, Y., 1999, "Predicting Progressive Delamination of Composite Material Specimens via Interface Elements," *Mech. Comp. Mat. Struct*., **6**, pp. 301-317.

Cook, R.D, Malkus, D.S, and Plesha, M.E, 2001, *Concepts and Applications of Finite Element Analysis*, Third Edition, John Wiley & Sons.

Diehl, T., 2008, "On Using a Penalty-Based Cohesive-Zone Finite Element Approach, Part I: Elastic Solution Benchmarks," *Int. J. Adhesion & Adhesives*, **28**, pp.237-255.

Dugdale, D.S., 1960, "Yielding of Steel Sheets Containing Slits," *J. Mech. Phys. Solids*, **8**, pp. 100–104.

Foulk, J.W., Allen, D.H., and Helms, K.L.E., 2000, "Formulation of a Three-Dimensional Cohesive Zone Model for Application to a Finite Element Algorithm," *Comput. Methods Appl. Mech. Engrg.*, **183**, pp. 51-66.

Gao, Y.F., and Bower, A.F., 2004, "A Simple Technique for Avoiding Convergence Problems in Finite Element Simulations of Crack Nucleation and Growth on Cohesive Interfaces," *Mod. Sim. Mater. Sci. Engrg.*, **12**, pp. 453-463.

Glaessgen, E.H., Saether, E., Phillips, D.R., and Yamakov, V., 2006, "Multiscale Modeling of Grain-Boundary Fracture: Cohesive Zone Models Parameterized from Atomistic Simulations," *Proceedings of the 47th AIAA/ASME/ASCE/AHS/ASC Structures, Structural Dynamics, and Materials Conference*, AIAA-2006-1674-CP, Newport, RI, May 1-4.

Goyal, V.K., Johnson, E.R., Davila, C.G., and Jaunky, N., 2002, "An Irreversible Constitutive Law for Modeling the Delamination Process Using Interface Elements," NASA/CR-2002-211758.

Gustafson, P.A., and Waas, A.M., 2008, "Efficient and Robust Traction Laws for the Modeling of Adhesively Bonded Joints," *Proceedings of the 49th AIAA/ASME/ASCE/AHS/ASC Structures, Structural Dynamics, and Materials Conference*, AIAA 2008-1847, Schaumburg, IL.

Hamitouche, L., Tarfaoui, M., and Vautrin, A., 2008, "An Interface Debonding Law Subject to Viscous Regularization for Avoiding Instability: Application to the Delamination Problems," *Eng. Fract. Mech.*, **75**, pp. 3084-3100.

Hilleborg, A., Modeer, M., and P., I.E., 1976, "Analysis of Crack Formation and Crack Growth in Concrete by Means of Fracture Mechanics and Finite Elements," *Cement & Concrete Res*., **6**, pp. 773-792.

Kem, K.S., McMeeking, R.M., and Johnson, K.I., 1998, "Adhesion, Slip, Cohesive Zones and Energy Fluxes for Elastic Spheres in Contact," *J. Mech. Phys. Solids*, **46**, pp. 243-266.

Klein, P. and Gao, H., 1998, "Crack Nucleation and Growth as Strain Localization in a Virtual-Bond Continuum," *Engr. Fract. Mech*, **61**, pp. 21-48.

Maugis, E., 1992, "Adhesion of Spheres – the JKR-DMT Transition using a Dugdale Model*," J. Colloid Interface Sci.*, **150**, pp. 243-269.

Needleman, A., 1987, “A Continuum Model for Void Nucleation by Inclusion Debonding,” *J. Appld. Mech*., **54**, pp. 525-531.

Needleman, A., 1990a, “An Analysis of Tensile Decohesion Along an Interface,” *J. Mech. Phys. Solids*, **38**, pp. 289–324.

Needleman, A., 1990b, “An Analysis of Decohesion Along an Imperfect Interface*,” Int. J. Fract*., **42**, pp. 21-40.

Nguyen, O. and Ortiz, M., 2002, “Coarse-Graining and Renormalization of Atomistic Binding Relations and Universal Macroscopic Cohesive Behavior,” *J. Mech. Phys. Solids*, **50**, pp. 1727-1741.

Oden, J.T., Prudhomme, S., Romkes, A., and Bauman, P., 2006, "Multi-scale Modeling of Physical Phenomena: Adaptive Control of Models," *SIAM Journal on Scientific Computing*, **28**, pp. 2359-2389.

Rabinovitch, O., 2008, “Debonding Analysis of Fiber-Reinforced-Polymer Strengthened Beams: Cohesive Zone Modeling versus a Linear Elastic Fracture Mechanics Approach,” *Eng. Fract. Mech.*, **75**, pp. 2842-2859.

Rice, J.R., 1992, “Dislocation Nucleation from a Crack Tip: An Analysis Based on the Peierls Concept,” *J. Mech. Phys. Solids*, **40**, pp. 239-271.

Rice, J.R., and Wang, J.S., 1989, “Embrittlement of Interfaces by Solute Segregation,” *Mat. Sci. Eng. A*, **107**, pp. 23–40.

Saether, E., 2008, “A Multiscale Methodology for Simulating Fracture in Polycrystalline Metals,” *PhD Thesis*, Virginia Polytechnic Institute and State University.

Schellekens, J.C.J., and de Borst, R., 1993, “On the Numerical Integration of Interface Elements,” *Int. J. Num. Meth. Engrg.*, **36**, pp. 43-66.

Segurado, J., and LLorca, J., 2004, “A New Three-Dimensional Interface Finite Element to Simulate Fracture in Composites,” *Int. J. Solids Struct.*, **41**, pp. 2977-2993.

Tomar, V., Zhai, J., and Zhou, M., 2004, “Bounds for Element Size in a Variable Stiffness Cohesive Finite Element Model,” *Int. J. Num. Meth. Engrg*., **61**, pp. 1894-1920.

Turon, A., Camanho, P., Costa, J., and Davila, C., 2004, “An Interface Damage Model for the Simulation of Delamination Under Variable-Mode Ratio in Composite Materials,” NASA/TM-2004-213277.

Turon, A., Davila, C.G., Camanho, P.P., and Costa, J., 2007, “An Engineering Solution for Mesh Size Effects in the Simulation of Delamination using Cohesive Zone Models,” *Eng. Fract. Mech*., **74**, pp. 1665-1682.

Tvergaard, V., 1990, "Effect of Fibre Debonding in a Whisker-Reinforced Metal," *Mat. Sci. and Eng. A*, **125**, pp. 203–213.

Tvergaard, V., and Hutchinson, J.W., 1992, "The Relation between Crack Growth Resistance and Fracture Process Parameters in Elastic–Plastic Solids," *J. Mech. Phys. Solids*, **40**, pp. 1377–1397.

Van den Bosch, M.J., Schreurs, P.J.G., and Geers, M.G.D, 2007, "A Cohesive Zone Model with a Large Displacement Formulation Accounting for Interfacial Fibrilation," *European J. Mech. A/Solids*, **26**, pp.1-19.

Xu, X.P., and Needleman, A., 1993, "Void Nucleation by Inclusion Debonding in a Crystal Matrix," *Mod. Sim. Mat. Sci. and Eng.*, **1**, pp. 111–132.

Yamakov, V., Saether, E., Phillips, D.R., and Glaessgen, E.H., 2006, "Molecular-Dynamics Simulation-Based Cohesive Zone Representation of Intergranular Fracture Processes in Aluminum," *J. Mech. and Phys. Solids*, **54**, pp. 1899-1928.

Zavattieri, P.D., Raghuram, P.V., and Espinosa, H.D., 2001, "A Computational Model of Ceramic Microstructures Subjected to Multi-Axial Dynamic Loading," *J. Mech. Phys. Solids*, **49**, pp. 27-68.

Zavattieri, P.D. and Espinosa, H.D., 2003, "An Examination of the Competition Between Bulk Behavior and Interfacial Behavior of Ceramics Subjected to Dynamic Pressure-Shear Loading," *J. Mech. Phys. Solids*, **51**, pp. 607-635.

Zhang, Z., Paulino, G.H., and Celes, W., 2007, "Extrinsic Cohesive Modelling of Dynamic Fracture and Microbranching Instability in Brittle Materials," *Int. J. Num. Meth. Engrg.*, **72**, pp. 893-923.

REPORT DOCUMENTATION PAGE

Form Approved
OMB No. 0704-0188

1. REPORT DATE *(DD-MM-YYYY)*	2. REPORT TYPE	3. DATES COVERED *(From - To)*
01-04-2009	Technical Memorandum	

4. TITLE AND SUBTITLE

The Development of Directional Decohesion Finite Elements for Mulstiscale Failure Analysis of Metallic Polycrystals

5a. CONTRACT NUMBER

5b. GRANT NUMBER

5c. PROGRAM ELEMENT NUMBER

6. AUTHOR(S)

Saether, Erik; Glaessgen, Edward H.

5d. PROJECT NUMBER

5e. TASK NUMBER

5f. WORK UNIT NUMBER

698259.02.07.07.03.01

7. PERFORMING ORGANIZATION NAME(S) AND ADDRESS(ES)

NASA Langley Research Center
Hampton, VA 23681-2199

8. PERFORMING ORGANIZATION REPORT NUMBER

L-19610

9. SPONSORING/MONITORING AGENCY NAME(S) AND ADDRESS(ES)

National Aeronautics and Space Administration
Washington, DC 20546-0001

10. SPONSORING/MONITOR'S ACRONYM(S)

NASA

11. SPONSORING/MONITORING REPORT NUMBER

NASA/TM-2009-215715

12. DISTRIBUTION/AVAILABILITY STATEMENT

Unclassified-Unlimited
Subject Category 26 Availability: NASA CASI (443) 757-5802

13. SUPPLEMENTARY NOTES

14. ABSTRACT

Atomistic simulations of intergranular fracture have indicated that grain-scale crack growth in polycrystalline metals can be direction dependent. At these material length scales, the atomic environment greatly influences the nature of intergranular crack propagation, through either brittle or ductile mechanisms, that are a function of adjacent grain orientation and direction of crack propagation. Methods have been developed to obtain cohesive zone models (CZM) directly from molecular dynamics simulation. These CZMs may be incorporated into decohesion finite element formulations to simulate fracture at larger length scales. A new directional decohesion element is presented that calculates the direction of Mode I opening and incorporates a material criterion for dislocation emission based on the local crystallographic environment to automatically select the CZM that best represents crack growth. The simulation of fracture in 2-D and 3-D aluminum polycrystals is used to illustrate the effectiveness of directional decohesion finite elements.

15. SUBJECT TERMS

Finite element method; Polycrystalline metals; Multiscale analysis

16. SECURITY CLASSIFICATION OF:			17. LIMITATION OF ABSTRACT	18. NUMBER OF PAGES	19a. NAME OF RESPONSIBLE PERSON
a. REPORT	b. ABSTRACT	c. THIS PAGE			STI Help Desk (email: help@sti.nasa.gov)
U	U	U	UU	45	19b. TELEPHONE NUMBER *(Include area code)* (443) 757-5802